Scientific Research Publishing

Journal of Modern Physics, 2018, 9, 2457-2472
http://www.scirp.org/journal/jmp
ISSN Online: 2153-120X
ISSN Print: 2153-1196

Ab-Initio Computations of Electronic, Transport, and Related Properties of Chromium Disilicide ($CrSi_2$)

Shaibu Onuche Mathias, Yuriy Malozovsky, Lashounda Franklin, Diola Bagayoko

Department of Mathematics and Physics, Southern University and A & M College, Baton Rouge, LA, USA
Email: cecemat4all@yahoo.com

How to cite this paper: Mathias, S.O., Malozovsky, Y., Franklin, L. and Bagayoko, D. (2018) *Ab-Initio* Computations of Electronic, Transport, and Related Properties of Chromium Disilicide ($CrSi_2$). *Journal of Modern Physics*, **9**, 2457-2472.
https://doi.org/10.4236/jmp.2018.914158

Received: November 17, 2018
Accepted: December 17, 2018
Published: December 20, 2018

Abstract

We report results from *ab-initio*, self-consistent density functional theory (DFT) calculations of electronic, transport, and related properties of chromium disilicide ($CrSi_2$) in the *hexagonal C*40 crystal structure. Our computations utilized the Ceperley and Alder local density approximation (LDA) potential and the linear combination of atomic orbitals (LCAO) formalism. As required by the second DFT theorem, our calculations minimized the occupied energies, far beyond the minimization obtained with self-consistency iterations with a single basis set. Our calculated, indirect band gap is 0.313 eV, at room temperature (using experimental lattice constants of a = 4.4276 Å and c = 6.368 Å). We discuss the energy bands, total and partial densities of states, and electron and hole effective masses. This work was funded in part by the US Department of Energy, National Nuclear Security Administration (NNSA) (Award No. DE-NA0003679), the National Science Foundation (NSF) (Award No. HRD-1503226), LaSPACE, and LONI-SUBR.

Keywords

Band Gap, BZW-EF Method, Density Functional Theory, Band Structure, $CrSi_2$

1. Introduction and Motivation

Chromium disilicide, $CrSi_2$, belongs to a list of semiconducting metal-silicides. It has a C40 hexagonal crystal structure, with a space group of $P6_222$ [1] [2] [3] [4], as depicted in **Figure 1(b)**. It is a highly degenerate p-type semiconductor with a narrow-forbidden band gap [5] [6]. $CrSi_2$ exists in several compositions [7] [8], ranging from 65.7% to 67.7% silicon [9]. The compound has three (3) formula

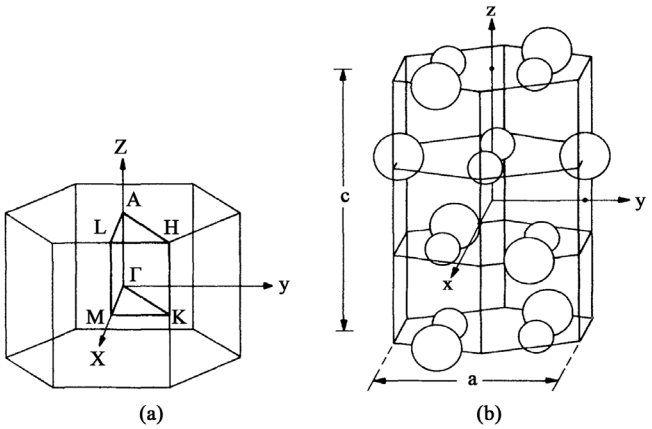

Figure 1. (a) Brillouin Zone for Hexagonal $CrSi_2$ and (b) Primitive unit cell of $CrSi_2$. Large spheres represent Cr atom positions while small spheres represent Si atom positions.

units per hexagonal unit cell [9]. It belongs to a group of semiconducting metal-silicides which have gained enormous attention in recent years, due to its properties and several areas of important applications. It has been the most studied representative of the metal-silicides since its initial characterization as a 0.35-eV bandgap semiconductor in the mid-1960's [10]. Due to the semiconducting nature and thermal stability of $CrSi_2$, it has special applications in optoelectronic devices, infrared detectors within silicon-based microelectronics components [3] [9] [11] [12]. $CrSi_2$, as a high-temperature compound, has been epitaxially grown on Si (111) substrate [1] [4] [13]. The preceding property of $CrSi_2$ makes it a potential material in the production of thermoelectric generators as well as for photovoltaic applications, in the middle of the infrared region [14]. As a narrow band gap semiconductor, $CrSi_2$ is a very good candidate in micro- and nano-electronics, respectively, and for photo-thermo converters and sensors [4] [15]. $CrSi_2$ belongs to a group of refractory silicides with a melting point at 1763 K, which makes it a potential candidate for high-temperature applications. $CrSi_2$ films are widely used in the area of new semiconductor device manufacturing due to their excellent electronic properties, high thermal stability, smooth surface and remarkable compatibility with the traditional silicon technique [12]. Krivosheeva *et al.* [16] reported that one of the most interesting and well investigated compounds is chromium disilicide which has the smallest lattice mismatch, as compared to other transition metal silicides [17] [18], with mono-crystalline silicon. $CrSi_2$ has a high electrical conductivity and a strong oxidation resistance which make it more attractive in microelectronics [12]. $CrSi_2$ is a potential candidate for optoelectronic devices, photo-voltaic cells, and thermoelectric conversion elements operating at elevated temperatures [1] [17] [19] [20] [21] [22].

Some experimental data have been reported for hexagonal $CrSi_2$. However, a consensus has not been reached, as far as its band gap is concerned; one reason for this situation stems from the lack of measured band gap values for bulk

$CrSi_2$. Bost *et al.* [9], in optical studies on well characterized $CrSi_2$ polycrystalline thin films, in 1988, obtained experimental results that provide evidence for the semiconducting nature of $CrSi_2$. Results from their measurements showed that $CrSi_2$ exhibits an indirect band gap of 0.35 eV [9]. Additionally, in a study of optical properties of $CrSi_2$, Henrion *et al.* [23] reported a band gap of 0.50 eV for $CrSi_2$ polycrystalline thin films, in 1992. Experimental studies of $CrSi_2$ films synthesized by high current Cr ion implantation resulted in band gap values of 0.7 eV and 0.84 eV [24] for $CrSi_2$ layers under different experimental conditions. Energy band gaps of 0.30 eV [25] to 0.35 eV [26] were obtained for $CrSi_2$ from Hall-effect measurements. Nishida [27] measured a band gap of 0.32 eV for $CrSi_2$ single crystals grown by using the floating zone melting technique. This author did not state whether the measured band gap was direct or indirect. Results from ellipsometry [28] suggested an indirect band gap of $Eg \leq 0.36$ eV for $CrSi_2$. All of the experimental band gaps reported so far for $CrSi_2$ are indirect except for the work of Nishida and of Galkin *et al.* [29]. While the former did not specify the nature of the gap, the latter found a direct band gap of 0.37 eV, for $CrSi_2$ epitaxial films. Clearly, results provided from past experimental works are not in total agreement. However, a general consensus points to a band gap in the range of 0.27 - 0.8 eV for various films of $CrSi_2$. **Table 1** shows experimental band gap values reported for $CrSi_2$.

Table 1. Results from Experimental Measurements of the Band Gap of Hexagonal $CrSi_2$. Except for the one indicated to be direct, all band gaps below are indirect. These band gaps are for films of various thicknesses, except the 0.32 eV band gap value estimated from the temperature dependence of resistivity for a single crystal.

Growth Or Measurement Method	E_g (eV)
Laser-assisted Synthesis of semiconductor chromium disilicide films	0.2[a]
Polycrystalline samples grown by amorphous thin films of Cr and Si in double electron-gun evaporation system.	0.27 ± 0.01[b]
Hall Effect measurements of Si-doped and Mn-modified $CrSi_2$ crystal	0.30 - 0.35[c]
Single crystals of $CrSi_2$ grown using the floating zone melting technique. Energy gap estimated from the temperature dependence of resistivity.	0.32[d]
Synchrotron Radiation Photoemission measurement of epitaxial $CrSi_2$ films prepared on Si (111) substrate at room temperature and 20K	0.32[e]
$CrSi_2$ films prepared by molecular beam epitaxy on $CrSi_2$ templates grown on Si (111) Substrate	0.34[f]
Polycrystalline thin films of $CrSi_2$ grown on silicon substrates (Samples annealed at 1100˚C)	0.35[g]
Ellipsometry of polycrystalline thin films of $CrSi_2$	≤0.36[h]
Optical absorption measurement of $CrSi_2$ thin films	0.35 - 0.5[i]
Transmittance and Reflectance Spectroscopy Study of A-type Epitaxial films 100nm thick grown by the Template method	0.37[j] direct
Optical Spectra measurement of $CrSi_2$ polycrystalline thin films	0.50[k]
Synthesis of $CrSi_2$ films by high current Cr ion implantation	0.7 and 0.8[l]

[a]Ref. [15], [b]Ref. [28], [c]Ref. [25] [26], [d]Ref. [27], [e]Ref. [30], [f]Ref. [31], [g]Ref. [9], [h]Ref. [28], [i]Ref. [23] [32], [j]Ref. [29], [k] Ref. [10], [l]Ref. [24].

Several theoretical calculations have been reported for the electronic structure of $CrSi_2$. While some of the calculations [31] have argued that $CrSi_2$ is semi-metallic in nature, others have predicted semiconductor properties for this material. Dasgupta *et al.* [4] obtained an indirect band gap of 0.35 eV, using the augmented spherical wave (ASW) method [33] [34] and the generalized gradient approximation (GGA) potential parameterized by Perdew *et al.* [35]. However, another calculation [20] performed with a similar method led to indirect and direct band gaps of 0.21 eV and 0.39 eV, respectively. Bellani *et al.* [28] reported a theoretical indirect band gap value of 0.38 eV using the linear-muffin-tin-orbital (LMTO) method, within the local density approximation (LDA). Two (2) calculations [19] [36] using the same method, within the local density approximation (LDA), obtained indirect band gaps of 0.29 eV and 0.25 eV, respectively. Another calculation [37], utilizing the LMTO method within the atomic spheres approximation (ASW), obtained a gap of 0.38 eV. L. F. Mattheiss [11] [38] reported an indirect band gap of 0.30 eV for bulk $CrSi_2$, using the linear augmented plane wave method (LAPW) and a local density approximation (LDA) potential. Mattheiss [39] used a scalar-relativistic version of the linear augmented-plane-wave (LAPW) method and obtained an indirect band gap of 0.30 eV. In another DFT calculation [16], with the full-potential linearized-augmented-plane-wave (FP-LAPW) led to an indirect band gap of 0.30 eV. A DFT approach, similar to the preceding, was applied in another calculation to obtain a band gap of 0.30 eV [10]. Zhou ShiYun *et al.* [12] obtained a gap of 0.353 eV in their study of optical properties of $CrSi_2$; they employed the plane-wave pseudo-potential method. Finally, recent DFT calculations performed in 2013 by Bhamu *et al.* [40] produced an indirect band gap of 0.28 eV for $CrSi_2$. The above calculation methods, potentials, and results are listed in **Table 2**.

Many of the results obtained from both experimental and theoretical calculations of $CrSi_2$ have been extensively reviewed in the preceding section. It is clear, however, from the contents of **Table 1** and **Table 2** that these results do not totally agree. While the disagreement can be seen among theoretical results, on the one hand, and between experimental results, on the other hand, there exists also a disagreement between experimental and theoretical results. This disagreement between theoretical results can be partly attributed to differences in computational methods. These disagreements strongly suggest that the correct band gap of bulk $CrSi_2$ is yet to be established unambiguously. This situation is a key motivation for our work. Also, the many current and potential applications of $CrSi_2$, as discussed at the beginning of this section, also motivated this work. These two motivations are supported by the fact that our method, to be discussed below, has led to the correct band gaps of well over 30 semiconductors. This method correctly predicted the band gap and related properties for more than three (3) semiconductors. Our aim, therefore, is to obtain accurately, through our BZW-EF, *ab-initio* self-consistent calculations, the true band gap as well as other electronic, transport and related properties of $CrSi_2$. Our BZW-EF *ab-initio*, self-consistent method has been successfully applied in several calculations

Table 2. Results from previous theoretical calculations of the band gap of hexagonal $CrSi_2$. except for the one indicated to be direct, all the gaps in the table are indirect.

Computational method	Potentials	E_g (eV)
Augmented-Spherical-Wave (ASW)	LDA	0.21[a]
Linear-Muffin-Tin-Orbital (LMTO)	LDA	0.25[b]
Linear Combination of Atomic Orbitals (LCAO)	LDA	0.28[c]
Semi-relativistic Linear Muffin-Tin-Orbital	LDA	0.29[d]
Linear Augmented-Plane-Wave (LAPW)	LDA	0.30[e]
Scalar Relativistic Linear Augmented-Plane-Wave	LDA	0.30[f]
Plane-Wave Pseudopotential Theory	LDA	0.353[g]
Full-Potential-Linearized-Augmented-Plane Wave (FL-APW)	LDA	0.35[h]
Semi-linear theory of relativity of the linear-muffin-tin-orbital (LMTO)	LDA	0.38[i]
Linear Muffin Tin Orbital (LMTO)	LDA	0.38[j]
Linear Augmented Plane Waves (LAPW)	GGA	0.30 (direct)[k]
Full-Potential-Linearized-Augmented-Plane Wave (FP-LAPW)	GGA	0.30[l]
Augmented Spherical Wave (ASW)	GGA	0.35[m]

[a]Ref. [20], [b]Ref. [19], [c]Ref. [40], [d]Ref. [36], [e]Ref. [11] [38], [f]Ref. [39], [g]Ref. [12], [h]Ref. [37], [i]Ref. [28], [j]Ref. [28], [k]Ref. [10], [l]Ref. [16], [m]Ref. [4].

[41]-[52] in the past and has proven to produce accurate properties of semiconductors. Therefore, this work is expected to follow in the same light.

2. Our Distinctive Method and Computational Details

Our computational method has been extensively discussed in previous publications [41]-[49], [53] [54] [55]. Two components of this method are commonly utilized in most calculations, *i.e.*, the choice of a density functional potential (LDA or GGA) and the linear combination of atomic orbitals (LCAO). Our software package actually employs the linear combination of Gaussian orbitals (LCGO). We selected the LDA potential of Ceperley and Alder, as parameterized by Vosko *et al.* [56] [57].

The distinctive feature of our method consists of our utilization of successive, self-consistent calculations, with augmented basis sets, in order to minimize the energy content of the Hamiltonian. This process ultimately leads to the absolute minima of the occupied energies (*i.e.*, the ground state), as required by the second theorem of density functional theory. This feature in our calculations is known as the Bagayoko, Zhao, and Williams (BZW) method [41] [58]-[63], as enhanced by Ekuma and Franklin (BZW-EF) [47] [48] [49] [54]. Unlike the BZW method, where orbitals representing unoccupied states are added in the order of increasing energies (in atomic or ionic species), the enhanced version (BZW-EF) adds, for a given principal quantum number, p, d and f orbitals, when applicable, before adding the corresponding s orbital. An orbital is applicable if it is occupied in any of the atomic species in the system. The BZW-EF

method reflects the realization [46] that polarization orbitals, for valence electrons, have primacy over the spherically symmetric s orbital [46] [47] [48] [49] [53] [55]. We describe below the actual implementation of the method using the program package developed at the Ames Laboratory of the US Department of Energy (DOE), Ames, Iowa [64] [65].

Our calculations for $CrSi_2$ started with a small basis set that was not smaller than the minimum basis set. This first self-consistent calculation was followed by Calculation II whose basis set was that of Calculation I as augmented with one orbital representing an excited state. Every augmentation of the basis set increases the dimension of the Hamiltonian by 2, 6, 10, or 14, depending on the s, p, d, or f character of the added orbital, respectively. We compared the self-consistent eigenvalues of the two calculations, graphically and numerically. Some occupied energies from Calculation II were lower than corresponding ones from Calculation I, as expected. After augmenting the basis set of Calculation II, Calculation III was performed self-consistently. The comparison of the occupied energies of Calculations II and III showed that some occupied energies of Calculation III were lower than corresponding ones from Calculation II. This process continued until three (3) consecutive calculations led to the same occupied energies, within our computational uncertainty of 5 meV, indicating that the ground state was reached. The first of the three (3) consecutive calculations was selected as the one providing the DFT description of the material; the basis set of this calculation is referred to as the *optimal basis set* [49]. As shown in the Section on results, this calculation was Calculation IV that produced the same occupied energies as V and VI. *The selection of the optimal basis set in the BZW-EF method is based on the crucial fact that the charge density from this calculation is the same one obtained in the calculations following it*. Hence, the Hamiltonian for this calculation, in light of the first theorem of DFT, is the same as those calculations following it, even though the Hamiltonian matrices will be different, given their different dimensions. Bagayoko [53] explained the reason the calculation with the optimal basis set is the one providing the DFT description of the material. Self-consistent iterations, up to the calculation producing the optimal basis set, yield eigenvalues that are due to interactions in the Hamiltonian. Calculations with basis sets larger than the optimal one and that contain the optimal one do not change the Hamiltonians or the occupied energies from their respective values obtained with the optimal basis set. However, these calculations can produce unoccupied energies that are lower than their corresponding values obtained with the optimal basis set. Given that the Hamiltonians of these calculations are the same as that obtained with the optimal basis set, the unoccupied energies lowered below their values obtained with the optimal basis no longer belong to the spectrum of the Hamiltonian, a unique functional of the charge density [53].

Computational details for this work follow. Chromium disilicide ($CrSi_2$) has a hexagonal C40 structure. It is in the space group of $P6_222$ $\left(D_6^4\right)$ [1] [2] [3] [4].

Its primitive cell contains a total of three (3) $CrSi_2$ formula units with individual atoms arranged as shown in **Figure 1(b)**. The space group is non-symmorphic, containing non-primitive translations ($\tau = \frac{c}{3}$ and $\frac{2c}{3}$) which interchange individual $CrSi_2$ layers [11] as in **Figure 1(b)**. Each Cr and Si atom in each of hexagonal layers of $CrSi_2$ has six (6) nearest neighbors at d = 2.557 Å. Each Cr and Si atom also has four (4) interplanar neighbors which are tetrahedrally coordinated. The hexagonal Bravais lattice for the primitive cell of $CrSi_2$ is generated from the primitive vectors: $\boldsymbol{t}_1$, $\boldsymbol{t}_2$ and $\boldsymbol{t}_3$, each described in Equation (1) as

$$\boldsymbol{t}_1 = (a/2)\left(\sqrt{3}\hat{i} - \hat{j}\right),\ \boldsymbol{t}_2 = a\hat{j},\ \boldsymbol{t}_3 = c\hat{k} \tag{1}$$

where a and c are the lattice constants. The internal atom position coordinates (ξ, ζ, η) for the primitive unit cell of $CrSi_2$ are in the units of the primitive vectors in Equation (1). These position coordinates of Cr and Si, within the hexagonal C40 primitive unit cell of $CrSi_2$, are given in **Table 3**, where x is the Si-atom position parameter. The position parameter of the Si-atom does not have an exact value. However, a value of $x = 1/6$ [64], corresponding to an ideal geometry [11], is normally used. In the ideal geometry, each Cr and Si atom has six nearest neighbors (d = 2.55 Å) [11], within each hexagonal $CrSi_2$ layer.

The standard hexagonal Brillouin zone for $CrSi_2$, as shown in **Figure 1(a)**, was generated from the reciprocal-lattice vectors that correspond to Equation (1). These reciprocal-lattice vectors are described by Equation (2) as given below.

Table 3. Position coordinates (ξ, ζ, η) of Cr and Si atom within the primitive unit cell of hexagonal C40 $CrSi_2$ in units of primitive vectors.

Atom	Site	ξ	η	ζ
Cr	3d	$\frac{1}{2}$	0	$\frac{1}{2}$
		0	$\frac{1}{2}$	$\frac{1}{6}$
		$\frac{1}{2}$	$\frac{1}{2}$	$-\frac{1}{6}$
Si	6j	x	$2x$	$\frac{1}{2}$
		$-x$	$-2x$	$\frac{1}{2}$
		$2x$	x	$\frac{1}{6}$
		$-2x$	$-x$	$\frac{1}{6}$
		x	$-x$	$-\frac{1}{6}$
		$-x$	x	$-\frac{1}{6}$

$$\boldsymbol{b}_1 = \left(4\pi/\sqrt{3}a\right)\hat{i},\ \boldsymbol{b}_2 = \left(2\pi/\sqrt{3}a\right)\left(\hat{i} + \sqrt{3}\hat{j}\right),\ \boldsymbol{b}_3 = \left(2\pi/c\right)\hat{k}, \quad (2)$$

where *a* and *c* are the lattice constants.

Our non-relativistic, self-consistent calculations were performed using room temperature (293K) experimental lattice constants [4] of a = 4.4284 Å and c = 6.36805 Å. We first performed *ab-initio* calculations for the ionic species, Cr^{2+} and Si^{-}, to generate input orbitals for the solid calculation. Our program package expanded the radial part of the atomic wave functions in terms of Gaussian functions by utilizing a set of even-tempered Gaussian exponents. For Cr^{2+}, our computations utilized 18, 18 and 16 even-tempered Gaussian exponents for the s, p, and d orbitals, respectively. For Si^{1-}, we utilized 18, 18 and 16 even-tempered Gaussian exponents for the s, p, and d orbitals, respectively. Our maximum exponent for Cr^{2+} is 1.1×10^5, while the minimum exponent is 0.317. Similarly, our maximum exponent for Si^{-} is 9.85×10^5, while the minimum exponent is 0.4045. Our computations utilized a mesh of 24 k-points in the irreducible Brillouin zone. However, in the band structure calculation, we utilized a total of 141 weighted k-points while a total of 144 weighted k-points was used in generating the energy eigenvalues for the electronic density of states. Self-consistency was reached after 60 iterations; then, the difference in potentials from any two consecutive calculation was equal to (or less than) 10^{-5}.

In the next section, we present results from our calculation of the band structure, density of states (DOS) and partial density of states (pDOS), and hole effective masses, respectively, using the LDA BZW-EF method.

3. Results

We list below, in Table 4, the valence orbitals in the successive calculations described above, along with the resulting band gaps. The orbitals in bold are the

Table 4. Successive, self-consistent calculations for $CrSi_2$, along with the valence orbitals and the resulting, indirect band gaps. The utilized room temperature lattice constants are a = 4.4284 Å and c = 6.36805 Å. Calculation IV, whose number is in bold in the first column, provided the DFT description of the material, with the corresponding, calculated, indirect band gap of 0.313 eV.

No	Chromium ($3Cr^{2+}$) ($1s^2\ 2s^2\ 2p^6$ ~ Core)	Silicon ($6Si^{1-}$) ($1s^2$ ~ Core)	No of Valence Functions	Indirect Energy Gap (eV) [L – M]
I	$3s^2\ 3p^6\ 3d^4$ **4p**	$2s^2\ 2p^6\ 3s^2\ 3p^3$	168	0.121
II	$3s^2\ 3p^6\ 3d^4$ **4p**	$2s^2\ 2p^6\ 3s^2\ 3p^3$ **4p**	204	0.162
III	$3s^2\ 3p^6\ 3d^4$ **4p 4d**	$2s^2\ 2p^6\ 3s^2\ 3p^3$ **4p**	234	0.295
IV	$3s^2\ 3p^6\ 3d^4$ **4p 4d 4s**	$2s^2\ 2p^6\ 3s^2\ 3p^3$ **4p**	**240**	**0.313**
V	$3s^2\ 3p^6\ 3d^4$ **4p 4d 4s**	$2s^2\ 2p^6\ 3s^2\ 3p^3$ **4p 4s**	252	0.314
VI	$3s^2\ 3p^6\ 3d^4$ **4p 4d 4s 5p**	$2s^2\ 2p^6\ 3s^2\ 3p^3$ **4p 4s**	270	0.318
VII	$3s^2\ 3p^6\ 3d^4$ **4p 4d 4s 5p**	$2s^2\ 2p^6\ 3s^2\ 3p^3$ **4p 4s 5p**	306	0.310

ones representing excited states. Calculation IV was the first one to produce the minima of the occupied energies; the same occupied energies were obtained with Calculations V and VI, signifying that these minima are the absolute ones and represent the ground state, as opposed to being local minima. Figure 2 shows the electronic energy bands for chromium disilicide, along with the bands from Calculations IV and V. As explained above, the two calculations result in the same occupied energies.

Figure 2 shows the electronic band structure of $CrSi_2$ as obtained with Calculation IV. The same figure shows the band structure from Calculation V. As stated above, the occupied energies from these calculations are identical. However, for conduction band energies above 4 eV, the two band structures are different, as explained in the Section on our distinctive, computational method.

Given the large number of bands immediately below and above the Fermi level, in Figure 2, a clear appreciation of their features is difficult. The magnified bands between −3 eV and +3 eV are shown in Figure 3 that provides a clearer view of the features of the DFT band structure in the vicinity of the Fermi level. In this figure, the valence band maximum (VB_{max}) is clearly at the L point, while the conduction band minimum (CB_{min}) is at the M point. The LDA BZW-EF calculated indirect band gap, from L to M, is 0.313 eV, while the smallest direct band gap, at L, is 0.517 eV. This value is only slightly smaller than the L to H and L to K indirect band gaps of 0.533 eV and 0.537 eV, respectively. The values of these gaps can be simply read in Table 5.

Table 5 lists the eigenvalues between −2.748 and +6.094 eV. We expect its content to be useful in comparisons of future experimental findings with our results. Such findings could include optical transition energies and band widths, among others.

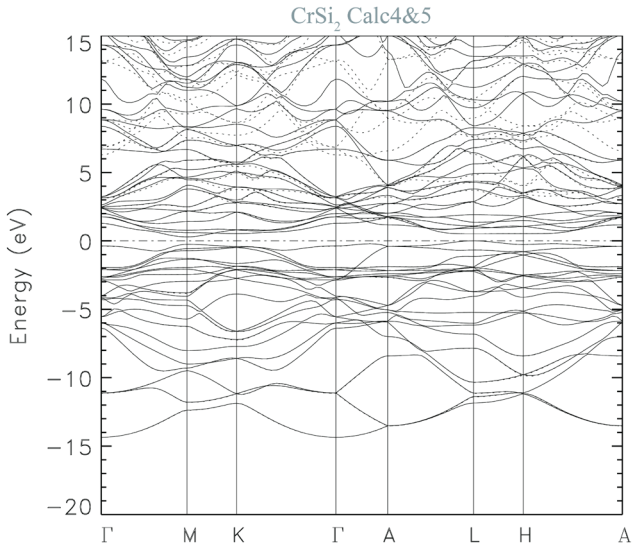

Figure 2. Graphical comparison of Calculations IV and V. Solid line represents Calculation IV while dotted lines represent Calculation V. The Fermi energy level is set at the zero point as denoted by the dashed line at the top of the valence band.

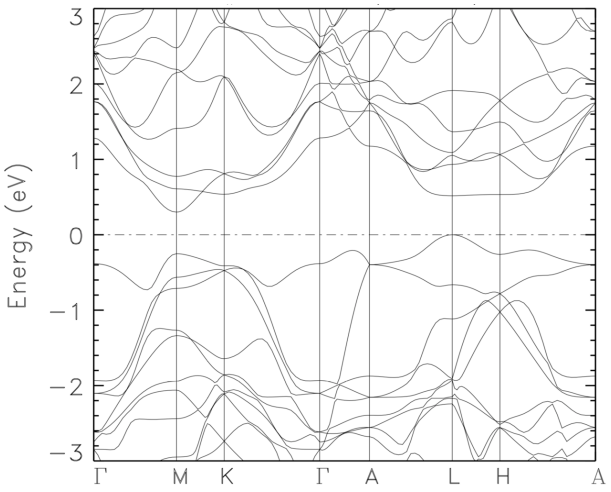

Figure 3. Electronic band structure of $CrSi_2$, as obtained from our ab initio calculations, using ours LDA BZW-EF optimal basis set of Calculation IV.

Table 5. Calculated electronic energies (in eV) of $CrSi_2$, between −2.748 and +6.094 eV, at the high symmetry points in the Brillouin zone, as obtained from Calculation IV. The Fermi energy is set equal to zero. Our calculated indirect band gap is 0.313 eV.

Γ-point	M-point	K-point	A-point	L-point	H-point
3.229	5.197	5.426	4.025	5.625	6.094
3.149	4.666	5.003	3.908	4.833	4.036
3.149	4.568	4.985	3.908	4.364	4.036
2.630	4.470	3.752	3.221	4.270	3.425
2.472	4.066	3.752	2.698	3.712	3.424
2.472	3.793	2.819	2.698	2.866	3.339
2.437	2.477	2.819	2.034	2.821	3.193
2.437	2.194	2.756	2.034	1.914	1.780
2.401	2.150	2.096	1.788	1.365	1.780
2.009	1.411	2.096	1.751	1.090	1.496
1.766	0.774	0.810	1.751	1.056	1.063
1.765	0.609	0.810	1.644	0.934	1.063
1.284	**0.313**	0.537	1.176	0.517	0.533
−0.383	−0.251	−0.411	−0.396	**0.000**	−0.260
−1.934	−0.563	−0.475	−0.397	−0.663	−0.782
−2.103	−0.711	−0.475	−1.874	−1.117	−0.782
−2.103	−1.266	−1.645	−2.155	−1.912	−1.024
−2.615	−1.339	−1.859	−2.155	−1.921	−1.024
−2.616	−1.943	−1.859	−2.394	−1.931	−2.481
−2.748	−2.061	−2.086	−2.557	−2.149	−2.516

The total density (DOS) and partial densities (pDOS) of states, shown in Figure 4 and Figure 5, respectively, provide further insight on the electronic structure. We employed the linear tetrahedron method [66] for the calculations of these densities of states, using the energy bands obtained with the optimal basis set, as shown in Figure 2. The broad peak features of the total density of states reflect the presence of three formula units per primitive cell. While both Cr and Si contribute to this feature between −5 and +5 eV, Si contributions clearly dominate outside this range, as per the partial densities of states. The calculated total width of the valence is 14.38 eV. The inset in Figure 4 shows a detailed view of the boundaries of the band gap.

We have calculated the electron effective masses, in the immediate vicinity of the minimum of the conduction band, at the M point and the hole effective masses, at the maximum of the valence bands, at M. Our calculated electron effective masses along *MΓ*, *MK*, and *ML* directions are 0.81, 0.77, and 1.38, respectively, in units of free electron mass (m_0). The calculated hole effective masses

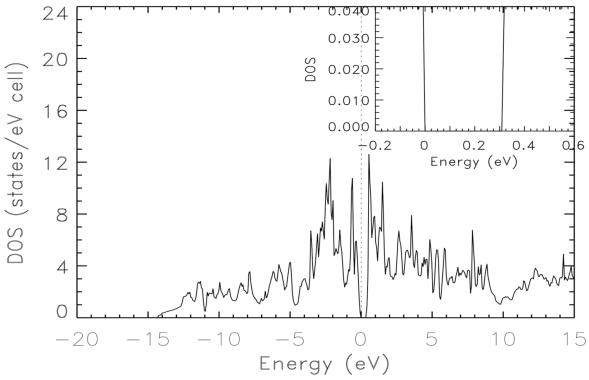

Figure 4. Results from the calculation of the density of states (DOS) for $CrSi_2$, as obtained using the bands from Calculation IV.

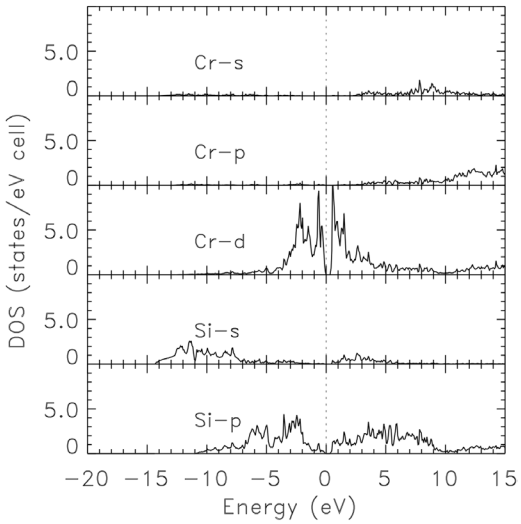

Figure 5. Results from the calculation of partial density of states (pDOS) for $CrSi_2$, as derived from the bands resulting from Calculation IV.

along *LA*, *LH*, *LM*, and *LΓ* axes are 1.3, 1.25, 1.19, and 1.07, respectively, in units of free electron mass. The electron and hole effective masses have been previously calculated by Mattheiss [11] who found that the components of the hole effective mass along *LA*, *LH*, and *LM* axes are 1.2 m_0, 1.3 m_0, 0.9 m_0, respectively. This author also reported electron effective masses of 0.7 m_0, 0.7 m_0, and 1.4 m_0, respectively. While our results for the electron effective masses are only slightly larger than or equal to the corresponding findings of Mattheiss, our hole effective masses, in the LA and LH directions, are much larger than those reported by Mattheiss. Our values somewhat are similar to those found by Mattheiss who used a completely different method (LAPW). Our calculated values for the effective masses are substantially smaller than the corresponding, empirical values of ~3 m_0 and ~20 m_0 for hole and electron effective masses, respectively, as determined from an analysis of transport data [25]. Clearly, more experimental measurements of effective masses in $CrSi_2$ are needed.

4. Discussion

There is a clear need for additional experimental studies of bulk $CrSi_2$. Indeed, as per the content of **Table 1**, only one (1) of the 11 experimental values for the band gap is for bulk $CrSi_2$. The author who reported this value of 3.2 eV did not specify whether the gap was direct or indirect. The other results are indirect band gaps for films of various thicknesses, fabricated by diverse growth techniques. In light of issues of quality of these films and in particular, the well-known quantum confinement effect, which tends to enlarge the gaps of films as compared to bulk materials, there is not much merit in comparing the calculated values for the bulk to these film gaps. The theoretical band gaps in **Table 2** are generally around 3.0 or 3.5 eV, except for the lower value of 0.21 eV and the negative one of −0.35 eV. Even though most of these theoretical results are not too far from the experimental one of 3.2 eV, the fact remains that our finding of 0.313 eV is the closest to this experimental finding. This agreement is partly explained in the Section on our method. Indeed, the BZW-EF method strictly adheres to the conditions of validity of a DFT calculation, *i.e.*, keeping the total number of particles constant and, verifiably, attaining the absolute minima of the occupied energies (the ground state) [53]. The latter condition is imposed by the second DFT theorem. As already noted, this condition is generally far from being met by results from self-consistent iterations with a single basis. A single basis set leads to a stationary solution among an infinite number of them. The relatively better agreement between our calculated band gap and the only experimental one for the bulk stems from the fact that our results possess the full physical content of DFT.

5. Conclusion

We have reported results for the ground state electronic structure and related properties of $CrSi_2$, using the BZW-EF method. Our LDA BZW-EF calculated

band gap of 0.313 eV is indirect. Our results for the band gap, total and partial densities of states, and the electrons and hole effective masses are expected to be confirmed by future experimental studies.

Acknowledgements

This research work was funded in part by the US Department of Energy, National and Nuclear Security Administration (NNSA) [Award No. DE-NA0003679], the US National Science Foundation (NSF) [Award No. HRD-1503226], LaSPACE, and LONI-SUBR.

Conflicts of Interest

The authors declare no conflicts of interest regarding the publication of this paper.

References

[1] Fathauer, R.W., Grunthaner, P.J., Lin, T.L., Chang, K.T., Mazur, J.H. and Jamieson, D.N. (1988) *Journal of Vacuum Science & Technology B: Microelectronics Processing and Phenomena*, **6**, 708-712. https://doi.org/10.1116/1.584352

[2] Vantomme, A., Nicolet, M.A., Long, R.G., Mahan, J.E. and Pool, F.S. (1993) *Applied Surface Science*, **73**, 146-152. https://doi.org/10.1016/0169-4332(93)90159-9

[3] Heck, C., Kusaka, M., Hirai, M., Iwami, M. and Yokota, Y. (1996) *Thin Solid Films*, **281**, 94-97. https://doi.org/10.1016/0040-6090(96)08583-5

[4] Dasgupta, T., Etourneau, J., Chevalier, B., Matar, S.F. and Umarji, A.M. (2008) *Journal of Applied Physics*, **103**, 113516. https://doi.org/10.1063/1.2917347

[5] White, A.E., Short, K.T. and Eaglesham, D.J. (1990) *Applied Physics Letters*, **56**, 1260-1262. https://doi.org/10.1063/1.103334

[6] Perumal, S., Gorsse, S., Ail, U., Prakasam, M., Chevalier, B. and Umarji, A.M. (2013) *Journal of Materials Science*, **48**, 6018-6024. https://doi.org/10.1007/s10853-013-7398-2

[7] Mason, K. N. (1981) *Progress in Crystal Growth and Characterization*, **2**, 269-307. https://doi.org/10.1016/0146-3535(81)90038-1

[8] Hansen, M. and Anderko, K. (1958) Constitution of Binary Alloys. 2nd Edition, McGraw-Hill, New York, p. 989.

[9] Bost, M.C. and Mahan, J.E. (1988) *Journal of Applied Physics*, **63**, 839-844. https://doi.org/10.1063/1.340078

[10] Krivosheeva, A.V., Shaposhnikov, V.L., Krivosheev, A.E., Filonov, A.B. and Borisenko, V.E. (2003) *Semiconductors*, **37**, 384-389. https://doi.org/10.1134/1.1568455

[11] Mattheiss, L.F. (1991) *Physical Review B*, **43**, 12549. https://doi.org/10.1103/PhysRevB.43.12549

[12] Zhou, S., Xie, Q., Yan, W. and Chen, Q. (2009) *Science in China Series G: Physics, Mechanics and Astronomy*, **52**, 46-51. https://doi.org/10.1007/s11433-009-0003-7

[13] Wetzel, P., Pirri, C., Peruchetti, J.C., Bolmont, D. and Gewinner, G. (1988) *Solid State Communications*, **65**, 1217-1220. https://doi.org/10.1016/0038-1098(88)90926-X

[14] Galkin, N.G. (2007) *Thin Solid Films*, **515**, 8179-8188.

https://doi.org/10.1016/j.tsf.2007.02.043

[15] Luches, A., Mulenko, S.A., Veiko, V.P., Caricato, A.P., Chuiko, V.A., Kudryavtsev, Y.V., Valerini, D., *et al.* (2007) *Applied Surface Science*, **253**, 6512-6516. https://doi.org/10.1016/j.apsusc.2007.01.023

[16] Krivosheeva, A.V., Shaposhnikov, V.L. and Borisenko, V.E. (2003) *Materials Science and Engineering*: *B*, **101**, 309-312. https://doi.org/10.1016/S0921-5107(02)00644-X

[17] Shiau, F.Y., Cheng, H.C. and Chen, L.J. (1986) *Journal of Applied Physics*, **59**, 2784-2787. https://doi.org/10.1063/1.336990

[18] Lange, H. (1997) *Physica Status Solidi* (*B*), **201**, 3-65.

[19] Halilov, S.V. and Kulatov, E.T. (1992) *Semiconductor Science and Technology*, **7**, 368. https://doi.org/10.1088/0268-1242/7/3/016

[20] Krijn, M.P.C.M. and Eppenga, R. (1991) *Physical Review B*, **44**, 9042. https://doi.org/10.1103/PhysRevB.44.9042

[21] Wolf, W., Bihlmayer, G. and Blügel, S. (1997) *Physical Review B*, **55**, 6918. https://doi.org/10.1103/PhysRevB.55.6918

[22] Zhou, F., Szczech, J., Pettes, M.T., Moore, A.L., Jin, S. and Shi, L. (2007) *Nano Letters*, **7**, 1649-1654. https://doi.org/10.1021/nl0706143

[23] Henrion, W., Lange, H., Jahne, E. and Giehler, M. (1993) *Applied Surface Science*, **70-71**, 569-572. https://doi.org/10.1016/0169-4332(93)90581-U

[24] Zhu, H.N. and Liu, B.X. (2000) *Applied Surface Science*, **161**, 240-248. https://doi.org/10.1016/S0169-4332(00)00303-2

[25] Nishida, I. and Sakata, T. (1978) *Journal of Physics and Chemistry of Solids*, **39**, 499-505. https://doi.org/10.1016/0022-3697(78)90026-4

[26] Shinoda, D., Asanabe, S. and Sasaki, Y. (1964) *Journal of the Physical Society of Japan*, **19**, 269-272. https://doi.org/10.1143/JPSJ.19.269

[27] Nishida, I. (1972) *Journal of Materials Science*, **7**, 1119-1124. https://doi.org/10.1007/BF00550193

[28] Bellani, V., Guizzetti, G., Marabelli, F., Piaggi, A., Borghesi, A., Nava, F., *et al.* (1992) *Physical Review B*, **46**, 9380. https://doi.org/10.1103/PhysRevB.46.9380

[29] Galkin, N.G., Maslov, A.M. and Konchenko, A.V. (1997) *Thin Solid Films*, **311**, 230-238. https://doi.org/10.1016/S0040-6090(97)00678-0

[30] Kim, K.H., Kang, J.S., Choi, C.K., Lee, J. and Olson, C.G. (1999) *Applied Surface Science*, **150**, 8-12. https://doi.org/10.1016/S0169-4332(99)00251-2

[31] Shugani, M., Aynyas, M. and Sanyal, S.P. (2015) *Journal of Experimental and Theoretical Physics*, **121**, 104-109. https://doi.org/10.1134/S1063776115060151

[32] Lange, H., Giehler, M., Henrion, W., Fenske, F., Sieber, I. and Oertel, G. (1992) *Physica Status Solidi* (*B*), **171**, 63-76.

[33] Williams, A.R., Kübler, J. and Gelatt Jr., C.D. (1979) *Physical Review B*, **19**, 6094. https://doi.org/10.1103/PhysRevB.19.6094

[34] Eyert, V. (2007) The Augmented Spherical Wave Method. In: *Lecture Notes in Physics*, Springer, Berlin Heidelberg.

[35] Perdew, J.P., Burke, K. and Ernzerhof, M. (1996) *Physical Review Letters*, **77**, 3865. https://doi.org/10.1103/PhysRevLett.77.3865

[36] Filonov, A.B., Tralle, I.E., Dorozhkin, N.N., Migas, D.B., Shaposhnikov, V.L., Petrov, G.V., *et al.* (1994) *Physica Status Solidi* (*B*), **186**, 209-215.

[37] Shaposhnikov, V.L., Krivosheeva, A.V., Krivosheev, A.E., Filonov, A.B. and Borisenko, V.E. (2002) *Microelectronic Engineering*, **64**, 219-223. https://doi.org/10.1016/S0167-9317(02)00788-8

[38] Mattheiss, L.F. (1991) *Physical Review B*, **43**, 1863. https://doi.org/10.1103/PhysRevB.43.1863

[39] Mattheiss, L.F. (1992) *Physical Review B*, **45**, 3252. https://doi.org/10.1103/PhysRevB.45.3252

[40] Bhamu, K.C., Sahariya, J. and Ahuja, B.L. (2013) *Journal of Physics and Chemistry of Solids*, **74**, 765-771. https://doi.org/10.1016/j.jpcs.2013.01.020

[41] Bagayoko, D., Zhao, G.L., Fan, J.D. and Wang, J.T. (1998) *Journal of Physics*: *Condensed Matter*, **10**, 5645. https://doi.org/10.1088/0953-8984/10/25/014

[42] Bagayoko, D., Franklin, L. and Zhao, G.L. (2004) *Journal of Applied Physics*, **96**, 4297-4301. https://doi.org/10.1063/1.1790064

[43] Bagayoko, D. and Franklin, L. (2005) *Journal of Applied Physics*, **97**, Article ID: 123708. https://doi.org/10.1063/1.1939069

[44] Jin, H., Zhao, G.L. and Bagayoko, D. (2007) *Journal of Applied Physics*, **101**, Article ID: 033123. https://doi.org/10.1063/1.2435802

[45] Stewart, A.D. (2015) *Journal of Advances in Physics*, **9**, 2277-2286. https://doi.org/10.24297/jap.v9i1.1463

[46] Franklin, L., Ekuma, C.E., Zhao, G.L. and Bagayoko, D. (2013) *Journal of Physics and Chemistry of Solids*, **74**, 729-736. https://doi.org/10.1016/j.jpcs.2013.01.013

[47] Ekuma, E.C., Franklin, L., Zhao, G.L., Wang, J.T. and Bagayoko, D. (2011) *Canadian Journal of Physics*, **89**, 319-324. https://doi.org/10.1139/P11-023

[48] Ekuma, C.E. and Bagayoko, D. (2011) *Japanese Journal of Applied Physics*, **50**, Article ID: 101103. https://doi.org/10.7567/JJAP.50.101103

[49] Ekuma, C.E., Jarrell, M., Moreno, J. and Bagayoko, D. (2012) *AIP Advances*, **2**, Article ID: 012189.

[50] Mbolle, A., Banjara, D., Malozovsky, Y., Franklin, L. and Bagayoko, D. (2017) *APS Meeting Abstracts*, **62**, 4.

[51] Banjara, D., Malozovsky, Y., Franklin, L. and Bagayoko, D. (2018) *AIP Advances*, **8**, Article ID: 025212. https://doi.org/10.1063/1.4996551

[52] Bamba, C.O., Malozovsky, Y., Franklin, L. and Bagayoko, D. (2016) *APS Meeting Abstracts*, **61**, 2.

[53] Bagayoko, D. (2014) *AIP Advances*, **4**, Article ID: 127104. https://doi.org/10.1063/1.4903408

[54] Nwigboji, I.H., Malozovsky, Y., Franklin, L. and Bagayoko, D. (2016) *Journal of Applied Physics*, **120**, Article ID: 145701. https://doi.org/10.1063/1.4964421

[55] Jin, H., Zhao, G.L. and Bagayoko, D. (2006) *Physical Review B*, **73**, 245214.

[56] Ceperley, D.M. and Alder, B.J. (1980) *Physical Review Letters*, **45**, 566. https://doi.org/10.1103/PhysRevLett.45.566

[57] Vosko, S.H., Wilk, L. and Nusair, M. (1980) *Canadian Journal of Physics*, **58**, 1200-1211. https://doi.org/10.1139/p80-159

[58] Nwigboji, I.H., Ejembi, J.I., Malozovsky, Y., Khamala, B., Franklin, L., Zhao, G. and Bagayoko, D. (2015) *Materials Chemistry and Physics*, **157**, 80-86. https://doi.org/10.1016/j.matchemphys.2015.03.019

[59] Diakite, Y.I., Traore, S.D., Malozovsky, Y., Khamala, B., Franklin, L. and Bagayoko,

D. (2017) *Journal of Modern Physics*, **8**, 531. https://doi.org/10.4236/jmp.2017.84035

[60] Zhao, G.L. and Bagayoko, D. (2000) *New Journal of Physics*, **2**, 16. https://doi.org/10.1088/1367-2630/2/1/316

[61] Bhandari, U., Bamba, C.O., Malozovsky, Y., Franklin, L.S. and Bagayoko, D. (2018) *Journal of Modern Physics*, **9**, 1773-1784. https://doi.org/10.4236/jmp.2018.99111

[62] Bagayoko, D. (2009) A Solution to the Band Gap Catastrophe: Predictive Calculations of Properties of Semiconductors and of Nuclei. *Proceedings of the First International Seminar on Theoretical Physics & National Development*, **1**, 15-35.

[63] Ekuma, C.E., Jarrell, M., Moreno, J. and Bagayoko, D. (2013) *Physics Letters A*, **377**, 2172-2176. https://doi.org/10.1016/j.physleta.2013.05.043

[64] Harmon, B.N., Weber, W. and Hamann, D.R. (1982) *Physical Review B*, **25**, 1109. https://doi.org/10.1103/PhysRevB.25.1109

[65] Feibelman, P.J., Appelbaum, J.A. and Hamann, D.R. (1979) *Physical Review B*, **20**, 1433. https://doi.org/10.1103/PhysRevB.20.1433

[66] Lehmann, G. and Taut, M. (1972) *Physica Status Solidi* (*B*), **54**, 469-477.